

Radio-frequency line-by-line Fourier synthesis based on optical soliton microcombs

BEICHEN WANG,^{1,†}  ZIJIAO YANG,^{1,2,†} SHUMAN SUN,¹ AND XU YI^{1,2,*}

¹Department of Electrical and Computer Engineering, University of Virginia, Charlottesville, Virginia 22904, USA

²Department of Physics, University of Virginia, Charlottesville, Virginia 22904, USA

*Corresponding author: yi@virginia.edu

Received 7 December 2021; revised 2 February 2022; accepted 4 February 2022; posted 9 February 2022 (Doc. ID 450103); published 11 March 2022

Radio-frequency (RF) waveform synthesis has broad applications in ultrawide-bandwidth wireless communications, radar systems, and electronic testing. Photonic-based approaches offer key advantages in bandwidth and phase noise thanks to the ultrahigh optical carrier frequency. In this work, we demonstrate Fourier synthesis arbitrary waveform generation (AWG) with integrated optical microresonator solitons. The RF temporal waveform is synthesized through line-by-line amplitude and phase shaping of an optical soliton microcomb, which is down-converted to the RF domain through dual-comb optical coherent sampling. A variety of RF waveforms with tunable repetition cycles are shown in our demonstration. Our approach provides not only the possibility of precise Fourier synthesis at microwave and millimeter-wave frequencies, but also a viable path to fully integrated photonic-based RF AWG on a chip. © 2022 Chinese Laser Press

<https://doi.org/10.1364/PRJ.450103>

1. INTRODUCTION

Fourier analysis creates one-to-one mapping between the temporal and frequency profiles of a waveform. Arbitrary temporal waveforms can be generated through Fourier synthesis by manipulating the spectral amplitude and phase in the frequency domain. Optical spectral waveshaping, or optical line-by-line waveshaping, has been widely applied to optical arbitrary waveform generation (AWG) [1,2], coherent control of quantum processes [3–5], and optical communications [6]. The broad optical bandwidth provides femtosecond temporal resolution in the Fourier synthesis [7] that is not attainable by conventional electronics.

Fourier synthesis in the optical domain can be down-converted to microwave and millimeter-wave frequencies [8–13] through the coherent dual-comb sampling method [14], and it could have wide applications in wireless communications, radar systems, and electronic testing [15–17]. When photomixing two optical frequency combs with different repetition rates on a photodiode, an RF frequency comb will be created, with its comb lines deriving their amplitudes and phases from the dual optical combs. Line-by-line amplitude and phase control on optical frequency combs [18] can then be coherently mapped to the RF frequency comb for waveform synthesis, which has been shown recently with electro-optic frequency combs [8–13]. Compared with other existing photonic methods for RF waveform generation [19–24], which rely on optical delay structures to either provide enough dispersion for

far-field frequency-to-time mapping, or route different replicas of a low repetition rate optical pulse to different arrival times on a photodiode, the Fourier synthesis method eliminates the need for long tunable optical delay lines and low repetition rate mode-locked lasers, and thus creates the potential for mass-scale integration on a photonic chip.

In this work, we demonstrate RF spectral line-by-line waveshaping and Fourier synthesis of RF waveforms by using optical dual-microresonator solitons [25–28]. The high repetition rate of soliton microresonator-based frequency combs (microcombs) [28] enables line-by-line amplitude and phase control of individual optical comb lines [18]. Dual-comb coherent sampling is then used to coherently down-convert the waveshaped optical microcomb to RF frequencies by beating it with another soliton microcomb on a fast photodiode. A complete discrete Fourier series can be constructed for waveform synthesis by nullifying the carrier envelope offset frequency in the down-converted RF frequency comb. A series of temporal waveforms, including tunable Gaussian, triangle, square, and “UVA”-like logo, is demonstrated to illustrate arbitrary waveform synthesis. All critical components in the dual-microcomb method, including soliton microcombs [28], wavelength multiplexers/demultiplexers [29], intensity and phase modulators [30], optical amplifiers [31], and ultrafast photodiodes [32], are compatible with photonic integration. A discussion of waveform quality and a comparison of the effective number of bits (ENOB) with electronic AWG are presented at the end of the manuscript.

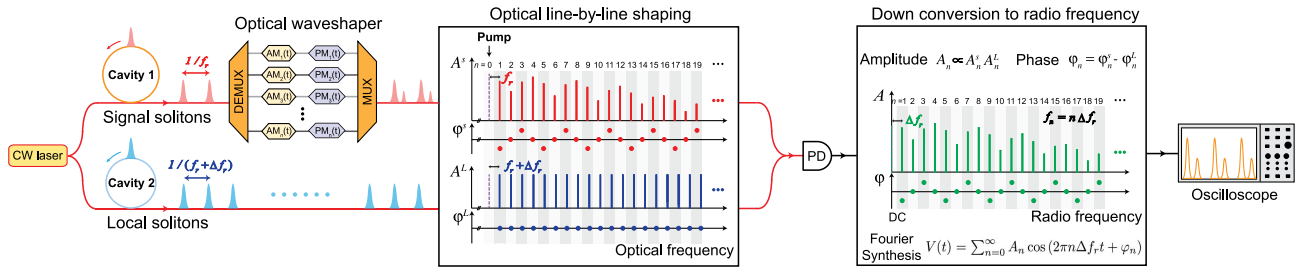


Fig. 1. Concept of RF line-by-line Fourier synthesis with dual-microresonator solitons. A radio-frequency (RF) comb that is composed of a series of equidistant RF lines is created by photomixing two soliton microcombs with slightly different repetition frequencies on a photodiode (PD). The RF comb spacing is set by the repetition rate difference of the two soliton microcombs, and the RF comb offset frequency is nullified by using a common pump laser to drive both optical solitons. To implement line-by-line amplitude (A_n) and phase (φ_n) control of the RF comb lines, one of the optical microcombs (signal solitons) goes through optical line-by-line waveshaping, and optical amplitude modulations (AMs) and phase modulations (PMs) are down-converted to the RF frequency comb through dual-microcomb coherent sampling. As the RF frequency comb forms a complete Fourier series, arbitrary temporal waveforms can be synthesized.

The concept of dual-microcomb RF line-by-line waveshaping is illustrated in Fig. 1. Signal solitons with repetition rate of f_r , and local solitons with repetition rate of $f_r + \Delta f_r$, are generated in two Kerr microresonators pumped by the same laser [33,34]. A radio-frequency (RF) comb with zero offset frequency and a comb spacing of Δf_r can be created by beating the signal and local solitons on a fast photodiode. The RF comb forms a Fourier series, with $V(t) = \sum_{n=0}^{\infty} A_n \cos(2\pi n \Delta f_r t + \varphi_n)$, where $V(t)$ is the voltage output of the photodiode, n is the comb line number, and A_n and φ_n are the amplitude and phase of the n th comb line, respectively. As the amplitude and phase of the RF comb lines are fully derived from the amplitude and phase of the corresponding optical comb lines, the line-by-line optical waveshaping on the signal solitons can fully control the amplitude and phase of the RF comb. In principle, dynamic waveform synthesis is possible by using time varying modulations of A_n and φ_n through the use of electro-optic modulators. Here, an off-the-shelf optical waveshaper is used instead to demonstrate static, repetitive waveform synthesis.

2. EXPERIMENTAL METHODS

In our experiment, the signal and local solitons are generated in SiN micro-ring resonators [35] with intrinsic quality factors of 7.7×10^6 and 4.3×10^6 , respectively. The radii of the signal and local soliton resonators are set to 228.65 μm and 228.30 μm , respectively, which introduces a 150 MHz repetition rate offset (Δf_r) between the two solitons. To create an RF comb with zero offset frequency, both optical solitons are generated using the same pump laser [33,34]. Thermoelectric coolers (TECs) are placed beneath microresonators to coarsely align the resonance frequencies of the two resonators at the pump laser wavelength. The thermal tuning of the resonant frequency is $\sim 2.5 \text{ GHz}/^\circ\text{C}$, and the TEC has a resolution of 0.01 $^\circ\text{C}$. A rapid laser frequency scanning method that leverages the single-sideband suppressed-carrier (SSB-SC) modulator [36] is used to generate single soliton states in both resonators simultaneously [34]. The pump frequency is controlled by the voltage-controlled oscillator (VCO) that drives the SSB-SC modulator, which scans over $\sim 3 \text{ GHz}$ in 150 ns from shorter to longer

wavelength. Figure 2(a) illustrates the simplified experimental setup. The optical spectra of signal (red) and local (blue) solitons are shown in Fig. 2(b). No active locking technique is used in our experiments for stabilization.

An optical line-by-line waveshaper [18] is used to control the phase of each comb line in the signal solitons (φ_n^S). The signal and local solitons are then combined in a 50/50 fiber coupler, and a second waveshaper is followed to control the amplitudes of each comb line pair (A_n^S, A_n^L). An erbium-doped fiber amplifier (EDFA) is used to amplify the solitons, and a high-speed, high-power photodiode converts the optical dual solitons into a zero offset RF frequency comb. The dual-comb optical spectrum after EDFA is measured on an optical spectrum analyzer, and an oscilloscope with 4 GHz bandwidth is used to characterize the RF temporal waveform, the spectrum of the RF comb, and the phase of the RF comb. Figure 2(c) presents the measurements when no phase or power adjustments are added by the waveshapers, except compensating for the dispersion introduced by optical fibers. This can serve as a reference point for line-by-line waveshaping in the RF domain. In our experiment, we purposely select a small RF comb spacing, $\Delta f_r = 150 \text{ MHz}$, such that the analog bandwidth of the RF comb will not exceed the 4 GHz bandwidth limit of our oscilloscope. The analog bandwidth in our experiment is limited by the oscilloscope, not by the Nyquist frequency of the coherent dual-comb sampling method [14] or the speed of the photodiode.

3. RESULTS

To illustrate line-by-line waveshaping in the RF domain, four types of Gaussian based temporal waveforms are demonstrated in Figs. 2(d)–2(g). The fundamental Gaussian waveform is shown in Fig. 2(d), which has a Gaussian envelope with flat phase in both the frequency and temporal domains. The power and phase of the generated RF comb match the designed ones very well, which are shown in red circles. The corresponding temporal waveform is a Gaussian pulse train with a time period of 6.71 ns, peak voltage of 0.94 V, and pulse width of 235 ps. No electrical amplifier after the photodiode is used in this work. The number of pulses in one period can be doubled by

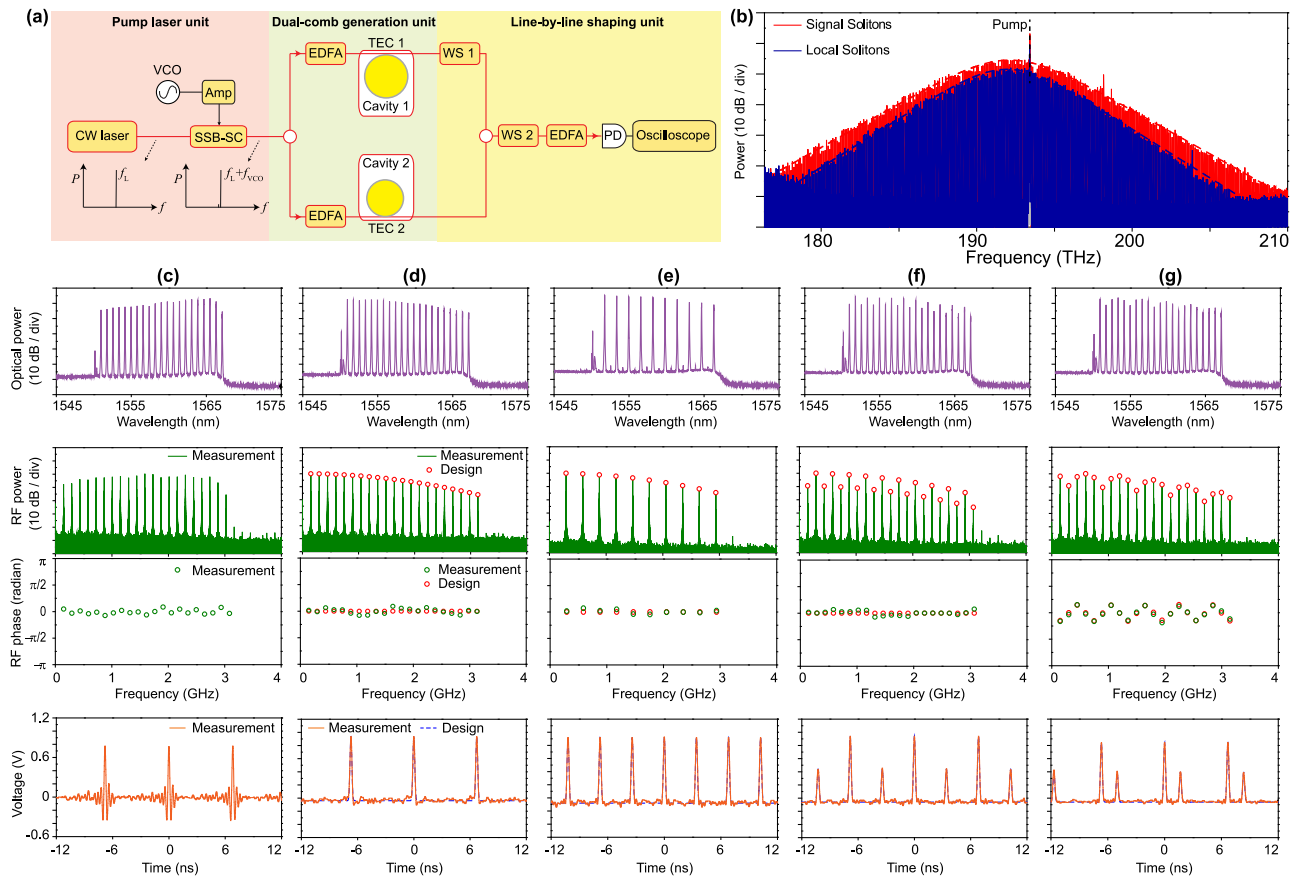


Fig. 2. Line-by-line waveshaping of RF Gaussian waveforms. (a) Simplified experimental setup. The pump laser frequency is derived from the frequency of a continuous-wave (cw) laser, f_L , and the voltage-controlled oscillator (VCO), f_{VCO} . (b) Optical spectra of the signal (red) and local (blue) microresonator solitons. Sech^2 envelope fittings are shown by dashed lines. The waveform synthesis is shown in (c)–(g) to illustrate the line-by-line control of the amplitude and phase of the RF comb. (c) Reference dual-microcomb waveforms with only dispersion compensation. (d) Amplitude control of the RF comb lines to shape temporal waveforms into Gaussian pulses with 235 ps pulse width. (e) Further amplitude control to add an equidistant Gaussian pulse and double the RF comb repetition frequency. (f) Adjust the relative Gaussian amplitudes through comb line amplitude control. (g) Combined amplitude and phase control of the RF comb to tune the relative position of the two Gaussian pulses. From top to bottom in each panel, we show (i) the optical spectra of soliton dual-microcomb after waveshaping, (ii) the down-converted RF spectra, (iii) the phase of RF comb lines, and (iv) the temporal waveforms. Designed comb line powers and phases are shown with red circles, and the designed temporal waveforms are shown with dashed blue lines.

knocking out half of the RF comb lines [Fig. 2(e)]. This is equivalent to adding an equidistant Gaussian pulse with the same amplitude in one temporal period. The amplitude of the added Gaussian pulse can be adjusted by changing the amplitude of the RF comb [Fig. 2(f)]. Finally, the temporal position of the added Gaussian pulse can be shifted by modifying both the amplitude and the phase of the RF comb lines [Fig. 2(g)]. The demonstration of these four Gaussian waveforms illustrates the full control of amplitude and phase in our RF line-by-line shaping method.

One direct application of line-by-line waveshaping is AWG. Three representative waveforms, including triangle, square, and “UVA”-like waveforms, are demonstrated here. For each temporal waveform, the corresponding amplitude and phase of each comb line can be derived by discrete Fourier transform of the temporal waveform. The Fourier transform of the triangle waveform is $x_{tr}(t) = \sum_{j=1}^{\infty} n^{-2} \cos[2\pi n \Delta f_r t + (-1)^j \pi/2]$, where j is the integer number, and $n = 2j + 1$.

The triangle waveform only has comb lines with odd number n , where the phase of the comb line alternates between $-\pi/2$ and $\pi/2$, and the amplitude decays quadratically with the line number n . These features are well reproduced in the power and phase spectra [Fig. 3(a)], and a triangle wave with period of 6.84 ns and 2.4 V peak to peak voltage is generated. Similarly, the square waveform is composed of comb lines with odd number: $x_{sq}(t) = \sum_{j=1}^{\infty} n^{-1} \cos(2\pi n \Delta f_r t - \pi/2)$. Figure 3(b) shows the measurements of the square waveform. Finally, a “UVA”-shaped waveform is shown in Fig. 3(c) to illustrate that the waveform construction in our method is arbitrary. All three demonstrated waveforms agree very well with the designed waveforms.

As the RF waveform repetition period is set by the repetition rate difference between the signal and local solitons, it can be tuned directly by adjusting the repetition rate of one of the solitons. Small range tuning of repetition period can be achieved by adjusting the temperature of the local soliton

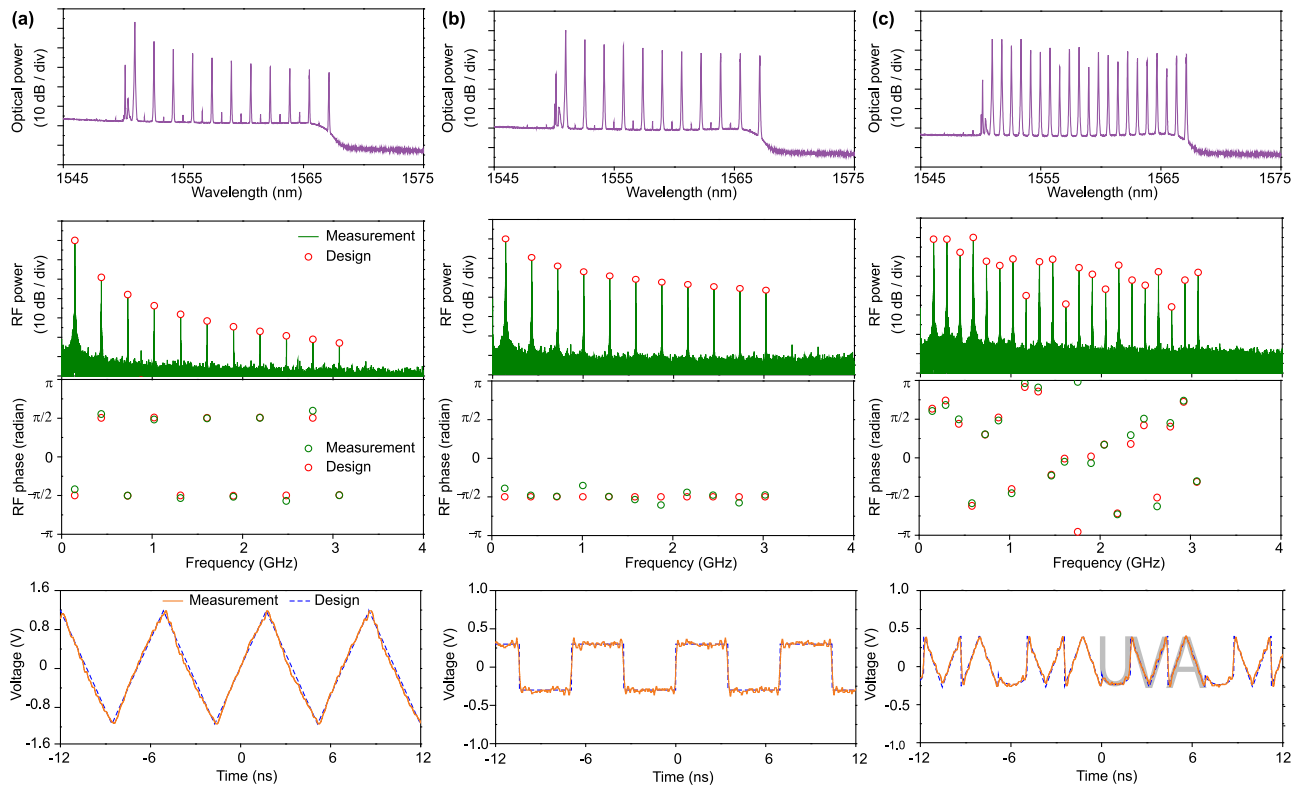


Fig. 3. Arbitrary waveform generation by using dual-microcomb RF Fourier synthesis. (a) Triangle waveform. (b) Square waveform. (c) “UVA”-like waveform. The corresponding (i) optical spectra, (ii) RF spectra, (iii) comb line phases, and (iv) temporal waveforms are shown from top to bottom in each panel. Designed comb line powers and phases are shown with red circles, and the designed temporal waveforms are shown with dashed blue lines.

microresonator. Figure 4(a) presents the RF comb repetition rate versus the temperature of the local soliton microresonator, and a tuning rate of ~ 30 MHz/ $^{\circ}\text{C}$ is measured. The spectra and temporal profiles of two Gaussian waveforms at (I) 21.95°C and (II) 22.15°C are shown in Figs. 4(b) and 4(c), where a difference of 0.29 ns in the waveform repetition periods can be seen. Large change of waveform period can be achieved by generating local solitons in a microresonator with slightly different radius. The RF comb repetition rate changes from ~ 150 to ~ 85 MHz when the radius of the local soliton microresonator is varied from 228.30 to 228.53 μm . Finally,

Fig. 4(d) presents the Allan deviation of the RF comb repetition rate, which is subject to the pump laser frequency drift and environment temperature fluctuation in our free-running system.

4. DISCUSSION

An important figure of merit for RF AWG is the effective number of bits (ENOB) [37], which can be used to evaluate the waveform quality or the effective resolution of the waveforms. For our dual-comb AWG method, the fundamental limit of its

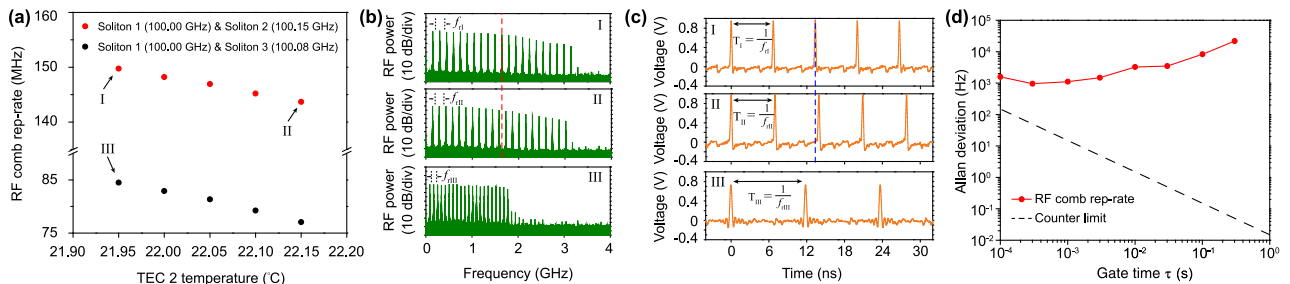


Fig. 4. Tuning the repetition frequency of the RF comb and temporal waveforms. (a) The RF comb repetition frequency is tuned by adjusting the repetition rate of local solitons. Small range tuning is realized by tuning the temperature of the local soliton microresonator with a thermoelectric cooler (TEC). Large range tuning is accomplished by generating local solitons in a microresonator with a slightly different radius. Soliton repetition rates are indicated in the figure legend. (b) and (c) show the electrical spectra and corresponding temporal waveforms at three different operating points indicated in (a). (d) Allan deviation of RF comb repetition rate at point I in (a).

ENOB is set by the optical power of the frequency combs. The fundamental limit of the ENOB in the dual-comb AWG method can be calculated using the ratio of signal voltage to the root-mean-square noise voltage fluctuations, and it is defined as $2^{\text{ENOB}} = V_p / \sqrt{2} V_\sigma$, where V_p is the time domain peak voltage, and V_σ^2 is the voltage noise variance. As harmonic distortion is not observed in our experiments, it is not included in our ENOB calculation. The digital quantization noise is not included either for our analog system. It should be noted that the widely used ENOB expression for sinusoidal waveforms [37] agrees with our definition when excluding harmonic distortion and digital quantization noise. For the sinc-shaped waveform, where all comb lines are shaped into equal power, the ENOB can be expressed as the following when the noise variance is dominated by shot noise (σ_S^2) and thermal noise (σ_T^2):

$$\begin{aligned} \text{ENOB} &= \frac{1}{2} \log_2 \left[\frac{V_p^2}{2R_{\text{load}}^2 (\sigma_S^2 + \sigma_T^2)} \right] \\ &= \frac{1}{2} \log_2 \left[\frac{2R^2 \cdot N^2 P_0^2}{(4e \cdot R \cdot NP_0 + k_B T / R_{\text{load}}) \cdot f_{\text{BW}}} \right], \quad (1) \end{aligned}$$

where we have used $V_p = 2R_{\text{load}} \cdot R \cdot NP_0$, $\sigma_S^2 = 4e \cdot R \cdot NP_0 \cdot f_{\text{BW}}$, and $\sigma_T^2 = k_B T / R_{\text{load}} \cdot f_{\text{BW}}$. R_{load} is the load resistance of the photodiode, R is the responsivity of the photodiode, N is the number of comb lines, P_0 is the optical power per comb line, e is the electron charge, k_B is the Boltzmann constant, T is the temperature, and f_{BW} is the total bandwidth. It can be seen that the ENOB increases with the total comb power (NP_0), but decreases with total bandwidth.

For Kerr soliton microcombs, the comb line power at the envelope center (P_c) can be expressed as [38] $P_c = (0.8814\eta/N)^2 \times P_p^{\text{min}}$, where P_p^{min} is the minimum pump power required for soliton existence, N is the number of one-sided comb lines in the 3 dB spectrum bandwidth, and $\eta = Q/Q_e$ is the waveguide to resonator loading factor. Q_e is the external or coupling Q -factor, and $Q = (Q_0^{-1} + Q_e^{-1})^{-1}$ is the total Q -factor (Q_0 is the intrinsic Q -factor). We can plot the fundamental limit of ENOB versus center comb line power (P_c) and the minimum pump power (P_p^{min}) for the sinc-shaped

waveform, where the optical power per comb line is shaped to half of the center comb line power ($P_0 = P_c/2$). In Fig. 5(a), the blue trace is obtained with the parameters of $\eta = 0.91$, $N = 20$, $f_{\text{BF}} = 50$ GHz, $R_{\text{load}} = 50 \Omega$, responsivity [32] $R = 0.8$ A/W, and 3 dB insertion loss (1 dB from phase and intensity modulators [30], 2 dB from the wavelength demultiplexer and multiplexer [39]) between the resonators and the photodiode. It can be seen that for comb line power below -10 dBm, the ENOB is affected by photodiode thermal noise, which can be addressed by using an optical post-amplifier to amplify the dual-comb power (red trace). A noise figure of 4 dB is assumed for the post-amplifier in the calculation of the ENOB. The ENOB of Keysight M8199A at 50 GHz is indicated with a dashed line in Fig. 5(a). It should be noted that ENOB for electronic AWG is typically measured for the sinusoidal waveform instead of the sinc waveform, and thus here it only serves as a rough reference for our photonic AWG analysis. The ENOB versus analog bandwidth is shown in Fig. 5(b) for center comb line power of 0 dBm (dashed) and -10 dBm (solid). The ENOB of our experiment (≈ 4) is much lower than the theoretical limit, because of the high loss in our optical path and the transmitted ASE noise from the pump EDFAs before microresonators. Both of these can be addressed in a fully integrated system.

The ultrahigh analog bandwidth has been the key advantage of photonic AWG systems. A 60 GHz analog bandwidth has been achieved previously using frequency-to-time mapping [19] and direct time-domain synthesis [23]. The analog bandwidth of the dual-comb Fourier synthesis method is ultimately limited by the Nyquist frequency of optical coherent sampling [14], i.e., half of the optical frequency comb repetition rate, and the bandwidth of the photodiode. The Nyquist frequency of dual-microcomb can range from a few gigahertz to a few hundred gigahertz [40,41]. The high Nyquist frequency has been applied to increase the bandwidth or sampling rate in dual-microcomb spectroscopy [27,33], Lidar [42,43], and imaging [44,45]. In terms of photodiodes, bandwidth exceeding hundreds of GHz has been demonstrated, and has been combined with soliton microcombs to generate RF signals with exceptional performance in power [46], phase noise [47,48], and

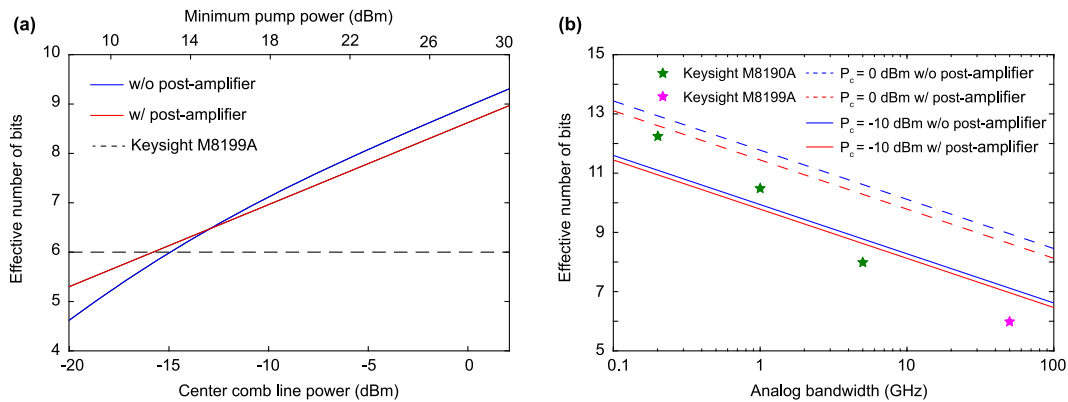


Fig. 5. Theoretical analysis of effective number of bits (ENOB). (a) Theoretical limit of dual-comb AWG ENOB versus the comb line power for 50 GHz analog bandwidth. The minimum pump power required to achieve such comb line power in the single soliton microcomb state is also shown. In this calculation, we assume 3 dB loss between the microresonators and the photodiode, and a 4 dB noise figure for the optical post-amplifier. (b) ENOB comparison of dual-comb AWG and state-of-the-art commercial electronic AWG.

time jitter [49]. It is thus possible to extend the analog bandwidth of dual-microcomb AWG beyond 100 GHz. In addition, all the critical components in dual-microcomb Fourier synthesis, including lasers, Kerr microresonators, multiplexers/demultiplexers, modulators, amplifiers, and ultrafast photodiodes, have been shown to be compatible with silicon photonics integration. Also, it eliminates the need for low-rate mode-locked lasers and long tunable delay lines required by the previous proposed on-chip solutions [19,23,24], and has the potential for mass production on a photonic chip. Finally, the time-bandwidth product (TBWP) of our current static arbitrary waveform demonstration is limited by the number of comb lines, which gives a maximum TBWP of 20. In contrast, a TBWP of 600 has been demonstrated by combining frequency-to-time mapping and optical interferometry [20]. In the future, the TBWP of our method can be increased dramatically by replacing the static waveshaper with phase and amplitude modulators for dynamic line-by-line phase and amplitude control [6,12,30], and the time aperture of the waveforms will be directly set by the time aperture of the modulation signals.

In summary, we have demonstrated arbitrary RF waveform generation through spectral line-by-line shaping with optical dual-microresonator solitons. In our experiment, the analog bandwidth of the waveform is 3 GHz, which is set purposely such that the waveform bandwidth will not exceed our oscilloscope bandwidth. The waveform analog bandwidth in our dual-microcomb method can be conveniently increased by adjusting the free spectral range (FSR) difference between the two soliton microresonators, which can be precisely controlled in microfabrication. In addition, although the demonstrated waveform generation is periodic and static, dynamic waveform generation can be implemented by using time varying amplitude and phase modulation of the optical comb lines through integrated photonic modulators [6,12,30].

Funding. National Science Foundation (2023775).

Acknowledgment. The authors thank Ligentec for resonator fabrication.

Disclosures. The authors declare no conflicts of interest.

Data Availability. Source data are available from the corresponding author upon reasonable request.

Code Availability. The codes that support the findings of this study are available from the corresponding author upon reasonable request.

†These authors contributed equally to this paper.

REFERENCES

- Z. Jiang, C.-B. Huang, D. E. Leaird, and A. M. Weiner, "Optical arbitrary waveform processing of more than 100 spectral comb lines," *Nat. Photonics* **1**, 463–467 (2007).
- S. T. Cundiff and A. M. Weiner, "Optical arbitrary waveform generation," *Nat. Photonics* **4**, 760–766 (2010).
- D. Goswami, "Optical pulse shaping approaches to coherent control," *Phys. Rep.* **374**, 385–481 (2003).
- M. C. Stowe, F. C. Cruz, A. Marian, and J. Ye, "High resolution atomic coherent control via spectral phase manipulation of an optical frequency comb," *Phys. Rev. Lett.* **96**, 153001 (2006).
- I. Barmes, S. Witte, and K. S. Eikema, "Spatial and spectral coherent control with frequency combs," *Nat. Photonics* **7**, 38–42 (2013).
- D. J. Geisler, N. K. Fontaine, T. He, R. P. Scott, L. Paraschis, J. P. Heritage, and S. Yoo, "Modulation-format agile, reconfigurable Tb/s transmitter based on optical arbitrary waveform generation," *Opt. Express* **17**, 15911–15925 (2009).
- H.-S. Chan, Z.-M. Hsieh, W.-H. Liang, A. Kung, C.-K. Lee, C.-J. Lai, R.-P. Pan, and L.-H. Peng, "Synthesis and measurement of ultrafast waveforms from five discrete optical harmonics," *Science* **331**, 1165–1168 (2011).
- V. Durán, S. Tainta, and V. Torres-Company, "Ultrafast electrooptic dual-comb interferometry," *Opt. Express* **23**, 30557–30569 (2015).
- V. Durán, P. A. Andrekson, and V. Torres-Company, "Electro-optic dual-comb interferometry over 40 nm bandwidth," *Opt. Lett.* **41**, 4190–4193 (2016).
- F. Ferdous, D. E. Leaird, C.-B. Huang, and A. Weiner, "Dual-comb electric-field cross-correlation technique for optical arbitrary waveform characterization," *Opt. Lett.* **34**, 3875–3877 (2009).
- X. Zhou, X. Zheng, H. Wen, H. Zhang, and B. Zhou, "Pair-by-pair pulse shaping for optical arbitrary waveform generation by dual-comb heterodyne," *Opt. Lett.* **38**, 5331–5333 (2013).
- F. Yin, Z. Yin, X. Xie, Y. Dai, and K. Xu, "Broadband radio-frequency signal synthesis by photonic-assisted channelization," *Opt. Express* **29**, 17839–17848 (2021).
- V. Ataie, D. Esman, B.-P. Kuo, N. Alic, and S. Radic, "Subnoise detection of a fast random event," *Science* **350**, 1343–1346 (2015).
- I. Coddington, W. Swann, and N. Newbury, "Coherent linear optical sampling at 15 bits of resolution," *Opt. Lett.* **34**, 2153–2155 (2009).
- J.-W. Lin, C.-L. Lu, H.-P. Chuang, F.-M. Kuo, J.-W. Shi, C.-B. Huang, and C.-L. Pan, "Photonic generation and detection of W-band chirped millimeter-wave pulses for radar," *IEEE Photon. Technol. Lett.* **24**, 1437–1439 (2012).
- P. Ghelfi, F. Laghezza, F. Scotti, G. Serafino, A. Capria, S. Pinna, D. Onori, C. Porzi, M. Scaffardi, A. Malacarne, V. Vercesi, E. Lazzari, F. Berizzi, and A. Bogoni, "A fully photonics-based coherent radar system," *Nature* **507**, 341–345 (2014).
- I. S. Lin, J. D. McKinney, and A. M. Weiner, "Photonic synthesis of broadband microwave arbitrary waveforms applicable to ultra-wide-band communication," *IEEE Microw. Wireless Compon. Lett.* **15**, 226–228 (2005).
- F. Ferdous, H. Miao, D. E. Leaird, K. Srinivasan, J. Wang, L. Chen, L. T. Varghese, and A. M. Weiner, "Spectral line-by-line pulse shaping of on-chip microresonator frequency combs," *Nat. Photonics* **5**, 770–776 (2011).
- M. H. Khan, H. Shen, Y. Xuan, L. Zhao, S. Xiao, D. E. Leaird, A. M. Weiner, and M. Qi, "Ultrabroad-bandwidth arbitrary radiofrequency waveform generation with a silicon photonic chip-based spectral shaper," *Nat. Photonics* **4**, 117–122 (2010).
- A. Rashidinejad and A. M. Weiner, "Photonic radio-frequency arbitrary waveform generation with maximal time-bandwidth product capability," *J. Lightwave Technol.* **32**, 3383–3393 (2014).
- A. Rashidinejad, D. E. Leaird, and A. M. Weiner, "Ultrabroadband radio-frequency arbitrary waveform generation with high-speed phase and amplitude modulation capability," *Opt. Express* **23**, 12265–12273 (2015).
- A. Rashidinejad, Y. Li, and A. M. Weiner, "Recent advances in programmable photonic-assisted ultrabroadband radio-frequency arbitrary waveform generation," *IEEE J. Quantum Electron.* **52**, 0600117 (2015).
- J. Wang, H. Shen, L. Fan, R. Wu, B. Niu, L. T. Varghese, Y. Xuan, D. E. Leaird, X. Wang, F. Gan, A. M. Weiner, and M. Qi, "Reconfigurable radio-frequency arbitrary waveforms synthesized in a silicon photonic chip," *Nat. Commun.* **6**, 5957 (2015).
- M. Tan, X. Xu, A. Boes, B. Corcoran, J. Wu, T. G. Nguyen, S. T. Chu, B. E. Little, R. Morandotti, A. Mitchell, and D. J. Moss, "Photonic rf arbitrary waveform generator based on a soliton crystal micro-comb source," *J. Lightwave Technol.* **38**, 6221–6226 (2020).

25. T. Herr, V. Brasch, J. Jost, C. Wang, N. Kondratiev, M. Gorodetsky, and T. Kippenberg, "Temporal solitons in optical microresonators," *Nat. Photonics* **8**, 145–152 (2014).
26. V. Brasch, M. Geiselmann, T. Herr, G. Lihachev, M. Pfeiffer, M. Gorodetsky, and T. Kippenberg, "Photonic chip-based optical frequency comb using soliton Cherenkov radiation," *Science* **351**, 357–360 (2016).
27. M.-G. Suh, Q.-F. Yang, K. Y. Yang, X. Yi, and K. J. Vahala, "Microresonator soliton dual-comb spectroscopy," *Science* **354**, 600–603 (2016).
28. T. J. Kippenberg, A. L. Gaeta, M. Lipson, and M. L. Gorodetsky, "Dissipative Kerr solitons in optical microresonators," *Science* **361**, eaan8083 (2018).
29. A. Rahim, J. Goyvaerts, B. Szelag, J.-M. Fedeli, P. Absil, T. Aalto, M. Harjanne, C. Littlejohns, G. Reed, G. Winzer, S. Lischke, L. Zimmermann, D. Knoll, D. Geuzebroek, A. Leinse, M. Geiselmann, M. Zervas, H. Jans, A. Stassen, C. Domínguez, P. Muñoz, D. Domenech, A. L. Giesecke, M. C. Lemme, and R. Baets, "Open-access silicon photonics platforms in Europe," *IEEE J. Sel. Top. Quantum Electron.* **25**, 8200818 (2019).
30. C. Wang, M. Zhang, X. Chen, M. Bertrand, A. Shams-Ansari, S. Chandrasekhar, P. Winzer, and M. Lončar, "Integrated lithium niobate electro-optic modulators operating at cmos-compatible voltages," *Nature* **562**, 101–104 (2018).
31. C. O. de Beeck, B. Haq, L. Elsinger, A. Gocalinska, E. Pelucchi, B. Corbett, G. Roelkens, and B. Kuyken, "Heterogeneous III-V on silicon nitride amplifiers and lasers via microtransfer printing," *Optica* **7**, 386–393 (2020).
32. Q. Yu, J. Gao, N. Ye, B. Chen, K. Sun, L. Xie, K. Srinivasan, M. Zervas, G. Navickaite, M. Geiselmann, and A. Beling, "Heterogeneous photodiodes on silicon nitride waveguides," *Opt. Express* **28**, 14824–14830 (2020).
33. A. Dutt, C. Joshi, X. Ji, J. Cardenas, Y. Okawachi, K. Luke, A. L. Gaeta, and M. Lipson, "On-chip dual-comb source for spectroscopy," *Sci. Adv.* **4**, e1701858 (2018).
34. B. Wang, Z. Yang, X. Zhang, and X. Yi, "Vernier frequency division with dual-microresonator solitons," *Nat. Commun.* **11**, 3975 (2020).
35. M. H. Pfeiffer, A. Kordts, V. Brasch, M. Zervas, M. Geiselmann, J. D. Jost, and T. J. Kippenberg, "Photonic damascene process for integrated high-Q microresonator based nonlinear photonics," *Optica* **3**, 20–25 (2016).
36. J. R. Stone, T. C. Briles, T. E. Drake, D. T. Spencer, D. R. Carlson, S. A. Diddams, and S. B. Papp, "Thermal and nonlinear dissipative-soliton dynamics in Kerr-microresonator frequency combs," *Phys. Rev. Lett.* **121**, 063902 (2018).
37. W. Kester, "Understand SINAD, ENOB, SNR, THD, THD+ N, and SFDR so you don't get lost in the noise floor," <https://www.analog.com/static/importedfiles/tutorials/MT-003.pdf> (2009).
38. X. Yi, Q.-F. Yang, K. Y. Yang, M.-G. Suh, and K. Vahala, "Soliton frequency comb at microwave rates in a high-Q silica microresonator," *Optica* **2**, 1078–1085 (2015).
39. J. F. Bauters, J. R. Adleman, M. J. Heck, and J. E. Bowers, "Design and characterization of arrayed waveguide gratings using ultra-low loss Si₃N₄ waveguides," *Appl. Phys. A* **116**, 427–432 (2014).
40. M.-G. Suh and K. Vahala, "Gigahertz-repetition-rate soliton microcombs," *Optica* **5**, 65–66 (2018).
41. Q. Li, T. C. Briles, D. A. Westly, T. E. Drake, J. R. Stone, B. R. Ilic, S. A. Diddams, S. B. Papp, and K. Srinivasan, "Stably accessing octave-spanning microresonator frequency combs in the soliton regime," *Optica* **4**, 193–203 (2017).
42. M.-G. Suh and K. J. Vahala, "Soliton microcomb range measurement," *Science* **359**, 884–887 (2018).
43. P. Trocha, M. Karpov, D. Ganin, M. H. Pfeiffer, A. Kordts, S. Wolf, J. Krockenberger, P. Marin-Palomo, C. Weimann, S. Randel, W. Freude, T. J. Kippenberg, and C. Koos, "Ultrafast optical ranging using microresonator soliton frequency combs," *Science* **359**, 887–891 (2018).
44. X. Yi, Q.-F. Yang, K. Y. Yang, and K. Vahala, "Imaging soliton dynamics in optical microcavities," *Nat. Commun.* **9**, 1 (2018).
45. C. Bao, M.-G. Suh, and K. Vahala, "Microresonator soliton dual-comb imaging," *Optica* **6**, 1110–1116 (2019).
46. B. Wang, J. S. Morgan, K. Sun, M. Jahanbozorgi, Z. Yang, M. Woodson, S. Estrella, A. Beling, and X. Yi, "Towards high-power, high-coherence, integrated photonic mmwave platform with microcavity solitons," *Light Sci. Appl.* **10**, 1 (2021).
47. S. Zhang, J. M. Silver, X. Shang, L. Del Bino, N. M. Ridler, and P. Del'Haye, "Terahertz wave generation using a soliton microcomb," *Opt. Express* **27**, 35257–35266 (2019).
48. T. Tetsumoto, F. Ayano, M. Yeo, J. Webber, T. Nagatsuma, and A. Rolland, "300 GHz wave generation based on a Kerr microresonator frequency comb stabilized to a low noise microwave reference," *Opt. Lett.* **45**, 4377–4380 (2020).
49. D. Jeong, D. Kwon, I. Jeon, I. H. Do, J. Kim, and H. Lee, "Ultralow jitter silica microcomb," *Optica* **7**, 1108–1111 (2020).